HHS Public Access

Author manuscript

*Adv Biosyst*. Author manuscript; available in PMC 2020 July 31.

Published in final edited form as:

*Adv Biosyst*. 2019 December ; 3(12): e1900184. doi:10.1002/adbi.201900184.

# Osterix-mCherry Expression Allows For Early Bone Detection In A Calvarial Defect Model

**Sara E. Strecker**[1], **Shimon Unterman**[1], **Lyndon F. Charles**[1], **Dmitry Pivovarchick**[3], **Peter F. Maye**[4], **Elazer R. Edelman**[1,2], **Natalie Artzi**[1,5,*]

[1]Massachusetts Institute of Technology, Institute for Medical Engineering and Science, 45 Carleton Street, E25-438, Cambridge, Massachusetts 02139, United States

[2]Cardiovascular Division, Brigham and Women's Hospital, Harvard Medical School, Boston, Massachusetts 02115, United States

[3]Ort Braude College, 51 Swallow Street, Karmiel, 2161002 Haifa, Israel

[4]Department of Reconstructive Sciences, University of Connecticut, Farmington, Connecticut 06032, United States

[5]Department of Medicine, Division of Engineering in Medicine, Brigham and Women's Hospital, Harvard Medical School, Boston, Massachusetts 02115, United States

## Abstract

The process of new bone formation following trauma requires the temporal recruitment of cells to the site, including mesenchymal stem cells, preosteoblasts, and osteoblasts, the latter of which deposit minerals. Hence, bone repair, a process that is assessed by the extent of mineralization within the defect, can take months before it is possible to determine if a treatment was successful. Here we use a fluorescently tagged Osterix, an early key gene in the bone formation cascade, as a predictive measure of bone formation. Using a calvarial defect model in mice, we evaluated the ability to noninvasively track the Osterix transcription factor in an Osterix-mCherry mouse model as a measure for bone formation following treatment with recombinant human Bone-Morphogenetic-Protein 2 (rhBMP-2). We utilized two distinct delivery materials, an injectable nanocomposite hydrogel and a collagen sponge, that afford distinct release kinetics and found that cherry-fluorescent protein can be detected as early as two weeks following treatment. Osterix intensity correlates with subsequent bone formation and hence can serve as a rapid screening tool for osteogenic drugs or for the evaluation and optimization of delivery platforms.

### Keywords

bone regeneration; BMP-2; Osterix; imaging; scaffold; nanocomposite

* -corresponding author.

**Author Contributions Statement**: SES, SU and LFC and NA designed the experiments. SES, SU, LFC, and DP performed experiments. SES and NA wrote the manuscript. SES and PFM generated the Osterix-mCherry mice. ERE and NA supervised the project. All authors discussed the results and reviewed the manuscript.

## Introduction:

Recombinant human bone morphogenetic protein 2 (rhBMP-2) has been used extensively in the clinic to induce bone formation[1–6]. It is commonly used in lumbar spinal fusion, where a rhBMP-2-soaked collagen sponge is inserted between two vertebrae to encourage bone growth in the intervertebral space; it also has found applications in the repair of tissue defects and fractures[5,7–9]. This approach is not without challenges, however, due to the poorly targeted delivery of high dose growth factor which can result in exuberant or ectopic bone formation and even an increased cancer risk[10–12].

Extensive preclinical research has focused on developing novel biomaterials to better control the delivery of rhBMP-2 and further enhance bone formation in a safe manner. Some of these approaches focus on modifying the material to direct release, while others attempt to mimic the bone microenvironment in order to minimize the need for rhBMP-2[13–18]. Typically, outcomes for *in vivo* preclinical testing rely on measures of bone mineral deposition using X-ray or CT, which typically take at least 4 weeks to provide an early readout of efficacy, substantially hampering cycle time and costs during biomaterial iteration and optimization. More invasive and destructive techniques, such as histology, immunostaining, and gene expression analysis, can yield insights into earlier changes during the repair process, but are cumbersome and require sequential animal sacrifice. The costs, ethical concerns, and challenges in following longitudinal data without same-animal controls militate for the development of early non-invasive techniques to predict later bone mineralization of novel biomaterial designs for delivery of rhBMP-2.

Previous researchers have used single-photon emission computed tomography (SPECT) or positron emission tomography (PET) scans to obtain high resolution spatiotemporal monitoring of early mineralization by tracking incorporation of labeled diphosphonate and fluoride into mineralizing tissues[19–23]. These techniques allow for high resolution three-dimensional imaging but are limited by the availability of specialized equipment, carry additional safety considerations, and require development of conjugated or radioactive reporters. Furthermore, these methods are limited to detecting low mineralization signals (by incorporation of a marker into the mineralizing tissue) but do not detect biological signals that precede mineralization and therefore make the differentiation of ectopic bone formation difficult.

The use of fluorescent mouse models in research has enabled noninvasive study of gene expression at a transcriptional level [24],[25]. The Osterix-mCherry mouse model affords the visualization of Osterix through a red fluorescent protein (monomeric Cherry)[26]. Osterix, a zinc finger transcription factor essential for early skeletal development and maintenance[27–29], is crucial for bone formation[30],[31],[32], and without it, a cartilaginous anlagen develops, but it does not mineralize[33].

The Osterix-mCherry mouse was created using Bacterial Artificial Chromosome (BAC) recombination-mediated genetic engineering (recombineering). A 40kb region of a BAC containing the Osterix gene and its upstream promoter region was combined with a monomeric cherry fluorescent protein, allowing for skeletal specificity without the

additional gene expression often seen with BAC mice[11]. By utilizing this skeletally specific fluorescent mouse model, early stages of osteogenesis can be elucidated by examining levels of cherry fluorescence[34]. We hypothesized that the Osterix mCherry mouse model combined with *in vivo* fluorescent imaging can be used as a screening tool for piloting new therapies for bone repair as mCherry expression is an indicator of early bone formation during normal skeletal development due to its linkage to the Osterix gene. Notably, the approach of using fluorescent reporters can be generalized to any specific biological signal that precedes a later functional output.

The goal of this approach is to allow for the rapid and cost-effective screening of biomaterial-mediated delivery of rhBMP-2. To evaluate the predictive power of this Osterix reporter on later mineralization, we directly compared the rhBMP-2-mediated repair of bilateral critical size calvarial defects in the mouse using two different biomaterial delivery systems. The first material was a collagen sponge in clinical use for delivery of rhBMP-2. The second, a nanocomposite hydrogel, was recently developed to provide controlled delivery of drugs to orthopedic tissues and is designed to release rhBMP-2 at a slower rate than the largely uncontrolled collagen sponge. By studying differential rhBMP-2 release kinetics, Osterix expression, and bone mineralization over time, we demonstrate that we can monitor bone formation via fluorescence weeks before mineralization is evident on μCT. We also show that material design and drug release kinetics affect the levels of Osterix mCherry fluorescence and eventual bone formation, as evidenced by Osteocalcin expression. This early view will allow us to track and to predict the kinetics of bone formation over time to reduce the cycle time needed when optimizing delivery systems for bone repair applications.

## Results:

### Osterix-Cherry mice allow for tracking of pre-osteoblastic / mesenchymal cells in vivo

The Osterix-mCherry mouse shows bright red fluorescence during all stages of skeletal development, even before mineralization, with the intensity increasing during differentiation. This model allows for tracking the kinetics of skeletal development over time and visualizing the mesenchymal and osteocytic cellular infiltration into the defect space, as well as the eventual correlation between fluorescence and differentiation. In designing the Osterix-mCherry mouse model, the cherry reporter was placed upstream of the second translational start site of the Osterix gene in order to allow for the visualization of both isoforms of Osterix[35,36] (Fig. 1A, red arrow). The founder lines were extensively characterized and showed high specificity toward skeletal elements as seen in a P2 mouse skull (Fig. 1B) and cortical section from an adult mouse (Fig. 1F). In the cortical section, there are three types of red-labeled cells; the osteocytes embedded within the bone, the osteoblasts on the bone surface and putative mesenchymal cells within the bone marrow near the cortical surface (Fig. 1F, blue arrows). These cell types are distinct and can be identified through morphology and location, though they have been extensively characterized in terms of gene and protein expression as well[37–40].

The mesenchymal cells make up approximately 2% of the nucleated cells within the marrow based on FACS sorting (Fig. 1G). These cells can be FACS isolated and plated. They go on to form red fluorescent colonies by 24 hours (Fig. 1C). If osteogenesis is induced in culture,

via adherence to the plastic of the culture dish, up to 80% of the cells gain red fluorescence as seen in the timeline (Fig. 1D and Supp. Fig. 1) and areas with the brightest fluorescence correspond to areas of von Kossa staining within the culture at day 21 (Fig. 1D, E), indicating that these cells are actively laying down mineral. Immunostaining for Osterix on tissue sections from the calvarial bone of adult mice show overlap between the immunostaining and the inherent fluorescent of the tissue (Fig. 1H, I), indicating that this model is accurately identifying cells which are expressing Osterix based on red fluorescence.

## Osterix-Cherry expression provides a read-out of putative bone formation before mineralization, and correlates with neo-osteogenesis

Bilateral 3.5mm defects were created in the calvarium of Osterix-mCherry mice using a dental drill[41]. Care was taken to maintain the periosteum and avoid the central suture. rhBMP-2 (0.2 μg) and saline were each pipetted onto collagen sponges (the delivery vehicle for rhBMP-2-mediated spinal fusion in the clinic) which had been cut to fit into the defect space (Fig. 2A, B). After closing, Osterix fluorescence was monitored weekly using IVIS Spectrum (In Vivo Imaging System, Perkin Elmer), and bone formation biweekly using μCT. Little to no mineralization appears at 2 weeks post-surgery (Fig. 2E, F) for mice treated with rhBMP-2, while a robust Cherry signal is seen on IVIS at 2 weeks in the defect space (Fig. 2C, D). To understand whether this indicates early neo-osteogenesis, tissue sections taken from rhBMP-2-treated Osterix-mCherry mice at 7 (Fig. 2G), 28 (Fig. 2H) and 56 days (Fig. 2I) post-surgery were characterized based on location relative to the bone surface and organization within the defect space. Mesenchymal cells are located adjacent to the bone surface. Osteoblasts are located on the bone surface and in some cases appear brighter. Osteocytes are strongly cherry-positive cells embedded in the bone surface. Cherry-positive cells are infiltrating into the critical size defect, which is denoted with the dashed line. A strong periosteal response[2,42] is seen and cherry–positive mesenchymal cells (MSC) start to migrate from the edges of the defect toward the center as early as 1 week, post-treatment (Fig. 2G). At 4 weeks, osteogenic cells start depositing new bone, and cherry-positive osteoblasts (OB) can be seen lining the newly formed bone surfaces, with MSCs still visible at 4 weeks. The onset of mineralization can be seen by 4 weeks on μCT (Fig. 5E) and at 8 weeks, much of the remodeling has taken place and the defect is often filled. Fewer MSCs are visible, and much of the cherry-positive cells become osteoblasts on the bone surface and osteocytes (OC), which are embedded in the new bone.

## The effects of differential biomaterial-mediated rhBMP-2 release profiles on Osterix expression and mineralization

Although early Osterix expression was clearly correlated with rhBMP-2 delivery and subsequent mineralization, it is not clear that this marker can distinguish between different rhBMP-2 release profiles and accurately predict the subsequent timing and degree of final mineralization. Calvarial defects were treated with rhBMP-2 loaded collagen sponges, as before, or a rhBMP-2 loaded nanocomposite (Fig. 3A). This nanocomposite is a hydrolytically degradable, two-component tissue-adhesive hydrogel composed of an oxidized polysaccharide (dextran aldehyde) and a polyamine (poly(amido amine) dendrimer); it has been extensively studied with respect to its tissue adhesive properties,

degradation properties, and drug release properties in the past[43–45]. The base hydrogel was further modified by addition of phyllosilicate nanoplatelets of two different aspect ratios to reinforce the mechanical and rheological properties of the hydrogel, as previously reported[46]. The nanocomposite's compressive modulus was approximately 200 kPa and the nanoplatelets adopted a well-distributed morphology in the material[46]. rhBMP-2 was loaded into the uncured macromer solution, which was then cured *in situ* in the calvarial defect; given the highly charged nature of the dendrimer and nanoplatelets, as well as the amine-reactive dextran macromers, it was expected that rhBMP-2 release would be substantially retarded in the nanocomposite compared to a collagen sponge.

We hypothesized that the different release kinetics would affect either the timing or the extent of mineralization and that the level of Osterix expression would allow us to predict those differences. Release profiles of rhBMP-2 from each material were studied *in vitro* (Fig. 3B). While the majority of rhBMP-2 was released from the collagen sponge within the first hour (87%), that same amount was released from the nanocomposites within 48 hours, confirming that rhBMP-2 delivery from nanocomposite was slower than in the collagen sponge.

When implanted in a calvarial defect, empty material controls evidenced very low Osterix-mCherry fluorescence (measured by IVIS at 4 and 8 weeks, Figs. 3 D, G, vs P, S respectively), and little to no mineralization (as quantified by μCT) (Figs. 3E, H, vs. Q, T), while the rhBMP-2-loaded biomaterials induced a robust Osterix and mineralization response which can be seen on IVIS after 2 weeks and via μCT after 4 weeks.

To correlate μCT data on bone mineralization, we assessed collagen deposition at 4 and 8 weeks post-surgery and bone volume fraction (BV/TV) at 8 weeks. Trichrome staining confirms that the nanocomposite persists in the defects 4 weeks post-surgery (Figs. 3I, O), however, by 8 weeks much of the nanocomposite has degraded (Fig. 3U, AA). As expected, the nanocomposite material (without rhBMP-2) showed a significantly reduced bone volume fraction (Fig. 3C), while both the rhBMP-2 groups showed higher BV/TV and bridging on histology. Bridging occurred in ~80% of the defects in the rhBMP-2-nanocomposite mice, compared to 60% in the rhBMP-2-collagen sponge group, which often also shows a small area of fibrous tissue (Fig. 3X, black arrow), indicating incomplete bridging.

### Osterix mCherry expression correlates with final bone mineral content.

Fluorescently tagged rhBMP-2 was tested in animals to determine the *in vivo* release kinetics of rhBMP-2 from either a collagen sponge or the nanocomposite. Figure 4A shows the fluorescent signal seen from the tagged rhBMP-2 in a calvarial defect model. The nanocomposite material shows a slower release with more rhBMP-2 retained especially early in the time-course. In the collagen sponge group, much of the rhBMP-2 is released after 1 hour as indicated by the high fluorescence level, whereas the nanocomposite group shows its highest fluorescence intensity at 24 hours. This is consistent with the burst release of rhBMP-2 seen by others[47–50]. Osterix-mCherry signal increased in the rhBMP-2-collagen sponge group until a peak at 2 weeks, followed by a decrease in signal until 8 weeks; in the rhBMP-2-nanocomposite group, the signal peaked at 4 weeks post-implantation (Fig. 4B). This is statistically significant at 4 and 8 weeks. rhBMP-2 retention

and Osterix-mCherry signal were correlated with mineralization by quantifying bone mineral content using μCT; bone content was higher in the rhBMP-2-nanocomposite group at 2, 4, and 8 weeks; both the collagen sponge and nanocomposite groups exhibited an increase in bone mineral content during defect repair (Fig. 4C). This is statistically significant throughout the entire time course; p value < 0.05. At 4 weeks, the Osterix-mCherry signal from the rhBMP-2-collagen sponge and the rhBMP-2-nanocomposite groups are strongly correlative with final bone mineral content (Fig. 4D), with a correlation coefficient of 0.74.

### rhBMP-2 loaded materials stimulate Osterix and Osteocalcin expression at 4 and 8 weeks

Osterix and Osteocalcin expression in regenerating bone tissues were confirmed through immunostaining at 4 and 8 weeks, with materials without rhBMP-2 acting as negative controls (Supp. Fig. 2). Using the Trichrome staining seen in Figure 3, we isolated a region at the edge of the original defect (Figs. 5A, B, C, D, highlighted in red) for immunostaining. In tissues where rhBMP-2 was added, there is a robust cellular response at 4 and 8 weeks. Red cells, in the form of Mesenchymal Stem Cells (MSC), Osteoblasts (OB) and Osteocytes (OC) can be seen in the defect space (Fig. 5E, F, G, H). Osterix expression was confirmed by immunostaining, which closely matched mCherry fluorescence (Fig. 5I, J, K, L). At both 4 and 8 weeks, the bony edge of the Osterix-Cherry calvarium is clearly visible as red osteocytes embedded within the matrix. and red osteoblasts on the bone surface. Mesenchymal stem cells (MSCs) are also visible at early time-points. MSCs can be identified by their location near, but not on, the bone surface within the marrow space or near the repairing defect. These cells can be differentiated from other bone cell types by their fibroblastic morphology. Osteoblasts can also be identified morphologically, as they are cuboidal and associated with the bone surface, often with a cobblestone like appearance. Osteoblasts are also osteocalcin positive, due to the amount of mineral they excrete. Osteocytes are identified by their location within the bone tissue and by long processes extending from the cell body. All these bone cell types are red fluorescent. Cell identity was confirmed histologically.

Osteocalcin expression was also confirmed through immunostaining. Osteocalcin is secreted by osteoblasts, binds hydroxyapatite, plays a role in mineral nucleation, and serves as a direct marker of new bone formation and mineralization[29,51,52]. Osteocalcin is not observed in the nanocomposite only controls at either 4 or 8 week (Supp. Fig. 2). In rhBMP-2 treated defects, an increasing osteocalcin signal can be detected at 4 and 8 weeks (Fig. 5M, N, O, P). This signal appears closest to where new bone is forming along the osteoblast surfaces and appears yellow due to the overlap with the Osterix-Cherry signal (see white arrows). Notably, the osteocalcin expression at 4 weeks in nanocomposite-treated defects was more modest than the expression in collagen sponges (Fig 5N), suggesting that new mineralization was more advanced in the collagen sponge condition at this time point despite the increased Osterix expression and 8 week mineral content in the nanocomposites.

## Discussion:

As researchers are working to develop therapeutics and delivery systems to induce bone formation, a need has arisen to find a way to test these therapeutics *in vivo*. Here, we demonstrate a facile method to predict late mineralization through the noninvasive tracking of biomarkers that herald bone repair. Currently, bone is assessed by the quantification of mineralization using μCT or X-ray, but it has become clear that the initiation of the bone formation process well precedes mineralization.

Healing of calvarial defects can rely on three potential reservoirs of progenitor cells in the periosteum, dura mater, and the cranial suture[53–56]. Each of these reservoirs stain positive for Osterix (Fig. 1B, H) and were preserved by the surgical technique, which intentionally spared the dura, defect-adjacent periosteum, and suture. While IVIS imaging alone did not provide adequate resolution to determine the localization and source of Osterix-upregulated cells during defect repair, immunofluorescence and histology supported a repair process that began at the circumference of the defect (Figs. 2G, 2H, 2I). This would suggest that the primary reservoir of progenitor cells to repair these defects was in the periosteum, as the dura mater was in contact with the entire defect area and the cranial suture was located medial to the defect.

During tissue repair, Osterix upregulation in progenitor cells and developing osteoblasts is an early indicator of bone formation. Typically, progenitor cells differentiate into osteoblasts which forms new bone, and these osteoblasts can become embedded in a matrix and ultimately differentiate into osteocytes[57]. Previous studies (Fig 1D) show that as these cells differentiate, the level of Osterix red fluorescence seen increases substantially, with osteocytes and osteoblasts showing the highest level of mCherry. We show here that high expression of Osterix is predictive of osteoblast formation and mineralization, and that this signal can be detected noninvasively using a fluorescent reporter. The increased Osterix-mCherry signal observed in rhBMP-2 treated defects (Figs. 3J, 3M, 3V, 3Y, 4B) may be attributed to either increased per-cell Osterix expression or a substantial migration and proliferation of Osterix positive progenitor cells. It is likely that this is a combination of the two; certainly, the initially acellular defect is infiltrated by a large number of Osterix positive cells during defect repair; however, histological time courses showed much more robust and widely distributed Osterix-mCherry expression during healing at 4 weeks than at 8 weeks (Figs. 2H, 2I, 5J, 5L), which correlated with IVIS signals (Fig. 4B). Crucially, the control conditions implanted without rhBMP-2 showed substantial cell infiltration but no concomitant increase in Osterix expression or mineralization (Fig. 3), supporting the role of rhBMP-2 in potentiating the recruitment and osteoblastic differentiation of progenitor cells in this model.

We tested our hypothesis that rhBMP-2-mediated mineralization could be predicted by early readouts of Osterix-mCherry signal using the clinical gold standard of an rhBMP-2-loaded collagen sponge, showing a strong correlation between Osterix-mCherry fluorescence and subsequent bone formation measured by μCT (Fig. 4D). By comparison with a biomaterial exhibiting delayed rhBMP-2 release kinetics and increased *in vivo* retention, we were able to correlate rhBMP-2 presentation with temporal changes in Osterix expression and final bone

mineral content. Although the underlying biomaterial systems were substantially different, rhBMP-2 negative controls of both materials showed poor endogenous healing, suggesting the materials were not themselves providing a confounding osteogenic signal. Of note, the fluorescence intensity (measured by radiant efficiency) seen in the nanocomposite reaches the same levels as those seen with rhBMP-2 on a collagen sponge, indicating this material is likely not impairing MSC infiltration or osteoblast differentiation. Temporal changes to Osterix expression were thus attributed to differences in rhBMP-2 presentation and release; these were in turn strongly correlated with final bone mineral content.

Sustained release of rhBMP-2, attained here when delivered from the nanocomposite, often results in a delayed but enhanced healing response[49,50,58]. This is likely due to the persistence of the growth factor causing an increase in its efficacy *in vivo*. rhBMP-2 burst release, from the collagen sponge, results in early stimulation of healing[49] (Fig. 3B) with the high levels of Osterix-mCherry expression at 2 weeks; this early stimulation was evident in the higher osteocalcin deposition noted in the collagen sponge at 4 weeks (Fig 5M). The enhancement in bone healing seen following sustained release of rhBMP-2 from the nanocomposite is likely due to enhanced activation and recruitment of progenitor cells[5], as indicated by the increase in Osterix-mCherry signal up to 4 weeks, followed by a gradual decline, yet higher than that seen for the collagen group even through 8 weeks (Fig. 4B, blue). This delayed Osterix upregulation was correlated with higher final bone mineral content and bone volume fraction (Figs. 4C, 3C). Previous studies have shown that rhBMP-2 is crucial for the differentiation of mesenchymal stem cells into osteocytes[49] and that the longer the cells are exposed to rhBMP-2, the more osteoblastic traits they express[3,52,59]. Because the nanocomposite provides a depot of rhBMP-2, unlike the collagen sponge, we were able to visualize differences in bone repair between the two systems.

By tracking temporal expression of a marker that precedes mineralization, it is possible to use Osterix signal as a predictive model; though this is most strongly correlative after 4 weeks. Ultimately, it will likely be a mix of detection techniques during the first 4 weeks of bone repair which will provide the most complete picture of the developing repair tissue (μCT, immunohistochemistry, IVIS, etc). Further study is needed to better understand the interplay between temporal presentation of osteogenic signals, cell infiltration and differentiation, and mineralization kinetics.

## Conclusions:

We developed a model system that allows for insight into the initial stages of bone repair, before definitive mineral deposition can be seen on either X-ray or μCT, using noninvasive fluorescence imaging. The Osterix-mCherry mouse model enables tracking recruited and differentiating MSCs before mineralization occurs and in the initial stages of bone repair. Quantification of bone formation at the molecular level allows us to gain insight into the interplay of progenitor cell recruitment and differentiation with mineralization. Osterix expression and eventual bone formation was dependent on rhBMP-2 release kinetics, in particular on the extent of sustained stimulation for recruitment and differentiation of MSCs into osteocytes, and hence can be used as a tool for the evaluation and optimization of osteogenic drug delivery platforms.

## Methods:

### Development of Dextran-Dendrimer Hydrogel Nanocomposite

A two-component material based on dextran aldehyde and generation-5 PAMAM dendrimer amine provides a cohesive hydrogel through aldehyde–amine cross-linking and an adhesive interface created by a dextran aldehyde-selective reaction with tissue amines. This hydrogel was augmented using two different aspect ratio nanoplatelets in our material. rhBMP-2 was added to the dextran such that the final concentration in the defect space was 0.2μg[46].

### Animal Care and Maintenance

Osterix-mCherry mice were generously provided the University of Connecticut. Transgenic animals were housed in a clean barrier facility and humanely treated in accordance with MIT institutional and IACUC guidelines.

### Calvarial Defect Surgeries

8–12 mice were used per experimental group. Mice were anesthetized with Ketamine/Xylazine and maintained on 0.5%−1% isoflurane. Bilateral, full thickness, non-suture-associated critical sized calvarial defects were induced in 16 week old Osterix-mCherry mice. A small incision (<1 cm) was be made in the skin above the midline of the skull. A 3.5–4 mm full thickness calvarial defect will be made with a diamond-coated trephine burr in the right and left parietal bone. The dura was left intact. Depending on the experimental group, defects were filled with an absorbable collagen sponge from an INFUSE bone graft kit (Medtronic), a PAMAM dendrimer/oxidized polysaccharide clay nanocomposite, collagen sponge infused with 0.2μg rhBMP-2 or nanocomposite with 0.2μg rhBMP-2. 3.5 mm diameter collagen sponges were created from a sheet of absorbable collagen sponge using a biopsy punch, while ~20 μl of nanocomposite was injected into the calvarial defect and allowed to cure *in situ*. rhBMP-2 was obtained from INFUSE bone graft kits (Medtronic), labeled as described below, and reconstituted in either hydrogel macromer solutions or as directed by the manufacturer prior to application to collagen sponges. Wounds were closed with sutures. Mice were medicated every 12 hours for the first 72 hours with 0.1mg/kg Buprenex for pain control.

### MicroCT imaging of bone growth

Mice were anesthetized with 1–2% isoflurane using a calibrated vaporizer inside an eXplore CT120 MicroCT (GE Healthcare) and noninvasively imaged for the extent and morphology of mineralization. Animals were imaged every 2 weeks, starting at week 2 and continuing for 8 weeks. Data was analyzed with Microview Software (Parallax Innovations, GE). A cylindrical region of interest 4mm by 4mm was created and aligned through the defect. Bone mineral content was measured using the Bone Analysis tool within the Parallax software suite. Auto-thresholding was set at 200 for all analyses performed.[60] Defects were classed as partially bridged if a single cross-section showed continuous mineralized bone from one side of the defect to another. If all cross-sections showed continuous mineralized bone, this was classed as fully bridged.

### IVIS imaging of bone growth

Mice were shaved then anesthetized with 1–2% isoflurane using a calibrated vaporizer inside an IVIS Spectrum (PerkinElmer). Images were taken with a 14 second exposure time. The excitation filter used was the 605nM filter and the emission filter used was 660nM to correlate with mCherry fluorescence. Images were obtained weekly, with the first set of images taken 1 day post-surgery to allow for recovery time for the mice.

For rhBMP-2 fluorescence the exposure time was 0.5 seconds. The excitation filter used was 570nM and the emission filter was 640nM.

### rhBMP-2 release *in vitro and in vivo*

Nanocomposite discs loaded with 10 μg of fluorescently tagged rhBMP-2 (Alexa Fluor 594-NHS ester) were prepared from dextran and dendrimer solutions. In order to track rhBMP-2 release *in vitro*, the protein was tagged using the Alexa Fluor 594 succinimidyl ester (NHS ester) amine-reactive fluorophore. The protein and dye (1:5 molar ratio) were reacted in 0.1 M sodium bicarbonate buffer (pH = 8.3) for 1 h and protein-dye conjugate purified by extensive dialysis. Successful conjugation was confirmed by SDS-PAGE. The degradation rate of the materials was studied by conjugating fluorescent labels to both the dextran (Alexa Fluor 488 hydrazide) and dendrimer (Alexa Fluor 755 succinimidyl ester) components and following the release of these tagged polymers into PBS using a fluorescence microplate reader at 30 min, 1 h, 2 h, 6 h, 12 h 24 h, and daily thereafter for up to 4 weeks. To avoid fluorescence quenching, <5% of fluorescently tagged materials was used in the final hydrogels. Degradation was also followed by mass loss measurement and results were correlated with loss of fluorescence method as previously published[44]. Subsequently, the nanocomposites were incubated in phosphate buffer saline (PBS, Gibco) at 37 °C. Release buffer (1 mL) was sampled at different time points ranging from 0.5 – 72 h. At each time point, 750 μL of the PBS was removed and replaced with fresh media. The release of rhBMP-2 protein was tracked by fluorescence signal at 585/617 for (excitation/emission) using a fluorimeter. Results were compared to a standard curve of known rhBMP-2 concentration in order to calculate the protein mass released. Each sample was performed in triplicate. Empty nanocomposite discs were used to analyze any background fluorescent signal that may arise from the degradation of the materials over the experimental period.

### Histological Preparation of Tissue Samples

Skulls were dissected and fixed in 10% formalin buffered in PBS for 7 days at 4°C. Ten defects were acquired from the collagen sponge group, and 16 defects were acquired from all other groups. Tissues were decalcified in 0.1N HCl, 0.25% Glutaraldehyde in PBS for 7 days. Tissues were then placed in 30% sucrose overnight and finally embedded in Cryomedia (Thermo Scientific). Frozen 8um sections were obtained using a Leica Cryostat and Cryofilm type II tape transfer system (Section-Lab Co. Ltd.). Sequential tissue sections were mounted using 50% glycerol buffered in PBS for imaging.

### Safranin O Staining

Sections were dried sections for 10 mins, then hydrated with distilled water for 5 mins. Sections were stained with Wiegert's iron hematoxylin working solution (Sigma) for 10

minutes. After staining, sections were washed in running tap water for 10 minutes then stained with fast green solution (0.05% Fast Green, Sigma) for 5 minutes. Next sections were quickly rinsed with 1% acetic acid solution for no more than 10 –15 seconds. Finally, sections were stained in 0.1% safranin O solution (Sigma) for 5 minutes. Sections were cleared with 95% ethyl alcohol for 2 minutes. Finally, sections were cover-slipped with a 50% glycerol, 50% PBS mixture.

### Masson's Trichrome Staining

First sections were kept overnight in Bouin's Solution (Sigma), then rinsed in running tap water for 5–10 minutes to remove the yellow color. Next they were stained with Wiegert's iron hematoxylin working solution for 10 minutes followed by a rinse in tap water for 10 minutes. Sections were washed in distilled water, then stained in Biebrich scarlet-acid fuchsin solution for 10–15 minutes. After another wash in distilled water, sections were placed into a phosphomolybdic-phosphotungstic (1:1) acid solution for 10–15 minutes then transferred directly to aniline blue solution and stained for 5–10 minutes. Sections were rinsed briefly in distilled water and de-stained in a 1% acetic acid solution for 2–5 minutes. Finally, sections were washed in distilled water and dehydrated quickly through 95% ethyl alcohol. Sections were cover-slipped with a 50% glycerol, 50% PBS mixture.

### DAPI staining

4',6-Diamidino-2-phenylindole (DAPI) was diluted to 1:10000 in PBS. Tissue sections were stained for 2–3 minutes in the dark then rinsed twice with PBS. Sections were cover-slipped with a 50% glycerol, 50% PBS mixture and imaged.

### Microscopy and Imaging

Whole mount images of embryonic animals were taken using a Zeiss SteREO Lumar V.12 fluorescent microscope at 9.6X magnification using the Cherry (HQ577/20 Ex, HQ640/40 Em) filter set (Chroma Technologies) and photographed with an Axiocam MRm digital camera (Zeiss). Cultures were imaged on a Zeiss Observer Z.1 microscope using the Cherry (HQ577/20 Ex, HQ640/40 Em, Q595lp beam splitter) filter set (Chroma Technologies).

Tissues were imaged on a Nikon Ti-E fluorescent microscope using a Coolsnap EZ digital camera (Photometrics). Filters used were DAPI (EX340–380, DM400, BD435–485), FITC (EX465–495, DM505, BA551–555), TRITC (HYQ545/30, HYQ 620/60) and Cy5 (HYQ620/60 Ex, HYQ700/75 Em)

### Immunostaining

Tissue sections were dried for 30 minutes at room temperature and then rehydrated by rinsing in PBS for 15 minutes. Aldehydes were quenched with 0.1% Glycine for 5 mins. Sections were then permeabilized for 30 minutes in 0.1% Triton X-100 (Sigma) at room temperature. Afterwards, sections were washed twice for 10 minutes in PBS at room temperature. Non-specific staining was blocked with a 1% BSA and 5% donkey or goat serum solution (Invitrogen) in PBS for one hour. The blocking solution was removed, and the section was incubated in an Osterix rabbit polyclonal IgG primary antibody (Santa Cruz Biotechnologies A-13, sc-22536) at a 1:300 dilution or a was a rabbit polyclonal to

Osteocalcin (ab93876) at a 1:100 dilution in 1% BSA and 1% serum in PBS overnight at 4°C. Tissue sections were then washed three times at 10 minutes per wash in PBS. Tissue sections were then suspended in a solution containing the secondary antibody, donkey anti-rabbit Alexa Fluor 488 (Invitrogen) or goat anti-rabbit Cy5 (Abcam) at a 1:100 dilution in 1% BSA and 1% donkey serum in PBS. Tissue sections were incubated with the secondary antibody at room temperature in the dark for two hours. Sections were then washed three times for ten minutes each in PBS and mounted on slides in 50% PBS-buffered glycerol for imaging.

## Preparation of Bone Marrow Stromal Cells for culture and FACS sort

3–4 week old Osterix-mCherry mice were sacrificed by $CO_2$ asphyxiation followed by cervical dislocation. Femurs and tibia were dissected. Bone marrow was collected through centrifugation. In brief, Eppendorf tubes, each containing a filter-less column, were prepared. 200ul of sterile cold PFE (98%PBS, 2%FBS, 2mM EDTA) were added to the bottom of the Eppendorf tube. Bones were spun at high speed for 3 minutes. Single cell suspensions were prepared by gently mixing the cells with a pipette followed by filtration through a 70-μm strainer. Cells which were to be analyzed immediately were subjected to a red blood cell lysis. For the red blood cell lysis, cells were pelleted and 1ml of Red Blood Cell Lysing Buffer (Sigma, R7757) was added to the pellet. This was gently mixed for one minute then placed on ice for three minutes. The Red Blood Cell Lysing Buffer was diluted with 10ml of PBS and then the cells were centrifuged at 350g for 7 minutes. The supernatant was decanted, and the cells were prepared for further profiling.

Cells which were to be cultured did not undergo Red Blood Cell Lysis and were plated at a density of $1.2 \times 10^6$ cells/cm$^2$ in DMEM culture medium containing 100 U/ml penicillin, 100 μg/ml streptomycin and 10% FCS (Hyclone). At day 4, the media was changed. In some cases, cells were cultured for a 21 day time period. In these cases, cells were grown in DMEM culture medium containing 100 U/ml penicillin, 100 μg/ml streptomycin and 10% FCS (Hyclone) for 7 days, with the media being changed on Day 4 and Day 7. On Day 7, the media was switched to αMEM and supplemented with 50 μg/ml ascorbic acid and 8 mM 2-glycerol phosphate and changed every two days until Day 21.

## FACS Analysis

Cultured cells were washed twice with cold PBS then digested with a mixture of 0.1% Collagenase P (Roche), 0.1% Hyaluronidase (Sigma), 2% FBS (Hyclone), 49% OPTI-MEM (Gibco) and 49% PBS (Gibco). Cells were digested for 10 minutes at 37C, scraped, then digested for an additional 5 minutes. The digestion was stopped using an equal amount of media containing 2% FBS, 49%PBS and 49% OPTI-MEM. Up to $10^7$ nucleated cells were resuspended in 500ul FACS staining buffer (PBS, 0.5% BSA, 2mM EDTA, pH7.2). Cells were analyzed on the FACS LSRII (BD) using the Red 649 nm Laser (670/30) and the YS 561 nm Laser (610/20, 600LP). The Blue 488 nm Laser (530/30, 505LP) was used to gate out auto-fluorescent cells.

### Statistical Analysis

All statistical analysis was performed using GraphPad Prism. Results are represented as mean +/− standard error. No animals were excluded from the analysis. Sample size for each individual experiment is shown in the figure legend. One-way ANOVA was performed on the bone volume fraction measurements in Figure 3C. Linear and non-linear regression analyses and Pearson correlation analyses were performed on IVIS and CT data sets in figure 4A, 4B and 4D. Paired students t-tests was performed on the data sets from Figure 4C. Statistical significance was defined as p value < 0.05.

## Supplementary Material

Refer to Web version on PubMed Central for supplementary material.

## Acknowledgements:

ERE was supported in part by a grant from NIH (R01 GM 49039) and some of the experiments by a sponsored research agreement from Sanofi. The authors acknowledge the assistance of other members of the Edelman lab, the *in vivo* imaging core at MIT, and the bio-medical engineering department at Sanofi.

## References:

[1]. Pimenta L, Marchi L, Oliveira L, Coutinho E, Amaral R, Journal of Neurologica Surgery, Part A: Central European Neurosurgery 2013, 74, 343.

[2]. Nakahara H, Takaoka K, Koezuka M, Sugamoto K, Tsuda T, Ono K, Clin Orthop Relat Res 1989, 299. [PubMed: 2912630]

[3]. Woo BH, Fink BF, Page R, Schrier JA, Jo YW, Jiang G, DeLuca M, Vasconez HC, DeLuca PP, Pharmaceutical Research 2001, 18, 1747. [PubMed: 11785696]

[4]. Mekhail AO, Bell GR, Seminars in Spine Surgery 2008, 20, 257.

[5]. Boerckel JD, Kolambkar YM, Dupont KM, Uhrig BA, Phelps EA, Stevens HY, García AJ, Guldberg RE, Biomaterials 2011, 32, 5241. [PubMed: 21507479]

[6]. Khosla S, Westendorf JJ, Oursler MJ, Journal of Clinical Investigation 2008, DOI 10.1172/JCI33612.

[7]. Oliveira L, Marchi L, Coutinho E, Abdala N, Pimenta L, World Spinal Column Journal 2010, 1, 19.

[8]. Adams R, Herrera-Nicol S, Jenkins A, Journal of Neurological Surgery Reports 2018, DOI 10.1055/s-0038-1667172.

[9]. Bodalia PN, Balaji V, Kaila R, Wilson L, Bone & Joint Research 2016, DOI 10.1302/2046-3758.54.2000418.

[10]. Joseph V, Rampersaud YR, Spine 2007, DOI 10.1097/BRS.0b013e31815b7596.

[11]. Gibbs DMR, Black CRM, Hulsart-Billstrom G, Shi P, Scarpa E, Oreffo ROC, Dawson JI, Biomaterials 2016, DOI 10.1016/j.biomaterials.2016.05.010.

[12]. Inoda H, Yamamoto G, Hattori T, International Journal of Oral and Maxillofacial Surgery 2007, DOI 10.1016/j.ijom.2006.07.011.

[13]. Sawyer AA, Song SJ, Susanto E, Chuan P, Lam CXF, Woodruff MA, Hutmacher DW, Cool SM, Biomaterials 2009, DOI 10.1016/j.biomaterials.2008.12.055.

[14]. Mariner PD, Wudel JM, Miller DE, Genova EE, Streubel SO, Anseth KS, Journal of Orthopaedic Research 2013, DOI 10.1002/jor.22243.

[15]. Lobo SE, Arinzeh TL, Materials 2010, DOI 10.3390/ma3020815.

[16]. Müller FA, Müller L, Hofmann I, Greil P, Wenzel MM, Staudenmaier R Biomaterials 2006, DOI 10.1016/j.biomaterials.2006.02.031.

[17]. Kim HD, Amirthalingam S, Kim SL, Lee SS, Rangasamy J, Hwang NS, Advanced Healthcare Materials 2017, DOI 10.1002/adhm.201700612.

[18]. Szpalski C, Wetterau M, Barr J, Warren SM, Tissue Engineering Part B: Reviews 2011, DOI 10.1089/ten.teb.2011.0427.

[19]. Rucher G, Cameliere L, Fendri J, Abbas A, Dupont K, Kamel S, Delcroix N, Dupont A, Berger L, Manrique A, Molecular Imaging and Biology 2018, DOI 10.1007/s11307-018-1202-2.

[20]. A.-M. C, J. L, N. A, R.B. A, A. P, C. G, D. L, C. C, F. R, G.Y. R, Acta Biomaterialia 2018, DOI 10.1016/j.actbio.2018.10.008.

[21]. Zhong ZA, Peck A, Li S, VanOss J, Snider J, Droscha CJ, Chang TA, Williams BO, Bone Research 2015, DOI 10.1038/boneres.2015.13.

[22]. P.S. L, S. M, A.-S. K, A. B, P. P, A. A, B.R. P, P. C, F.E. W, R. S, M. B, Scientific reports 2015, DOI 10.1038/srep10238.

[23]. Ventura M, Franssen GM, Oosterwijk E, Boerman OC, Jansen JA, Walboomers XF, Journal of Tissue Engineering and Regenerative Medicine 2016, DOI 10.1002/term.1862.

[24]. Vintersten K, Monetti C, Gertsenstein M, Zhang P, Laszlo L, Biechele S, Nagy A, Genesis 2004, 40, 241. [PubMed: 15593332]

[25]. Prasher DC, Trends in Genetics 1995, 11, 320. [PubMed: 8585130]

[26]. Fink D, Wohrer S, Pfeffer M, Tombe T, Ong CJ, Sorensen PHB, Genesis 2010, 48, 723. [PubMed: 20853428]

[27]. Liu Y, Strecker S, Wang L, Kronenberg MS, Wang W, Rowe DW, Maye P, PLoS ONE 2013, 8, DOI 10.1371/journal.pone.0071318.

[28]. a Kaback LEE, Soung DOY, Naik A, Smith N, Schwarz EM, Keefe RJO, Drissi H, Journal of cellular physiology 2008, 214, 173. [PubMed: 17579353]

[29]. Matsubara T, Kida K, Yamaguchi A, Hata K, Ichida F, Meguro H, Aburatani H, Nishimura R, Yoneda T, Journal of Biological Chemistry 2008, 283, 29119. [PubMed: 18703512]

[30]. Rashid H, Ma C, Chen H, Wang H, Hassan MQ, Sinha K, de Crombrugghe B, Javed A, Connective Tissue Research 2014, 55, 83. [PubMed: 25158187]

[31]. Kaback LA, Soung do Y, Naik A, Smith N, Schwarz EM, O'Keefe RJ, Drissi H, J Cell Physiol 2008, 214, 173. [PubMed: 17579353]

[32]. Hatta M, Yoshimura Y, Deyama Y, Fukamizu A, Suzuki K, Int J Mol Med 2006, 17, 425. [PubMed: 16465388]

[33]. Nakashima K, Zhou X, Kunkel G, Zhang Z, Deng JM, Behringer RR, De Crombrugghe B, Cell 2002, 108, 17. [PubMed: 11792318]

[34]. Renn J, Winkler C, Developmental Dynamics 2009, 238, 241. [PubMed: 19097055]

[35]. Milona M, Gough JE, Edgar AJ, BMC Genomics 2003, 4, 43. [PubMed: 14604442]

[36]. Strecker S, Fu Y, Liu Y, Maye P, Genesis 2013, 51, 246. [PubMed: 23180553]

[37]. Burr DB, Akkus O, in Basic and Applied Bone Biology, 2013, pp. 3–25.

[38]. Nakamura H, Journal of Hard Tissue Biology 2007, 16, 15.

[39]. Montesinos JJ, Flores-Figueroa E, Castillo-Medina S, Flores-Guzmán P, Hernández-Estévez E, Fajardo-Orduña G, Orozco S, Mayani H, Cytotherapy 2009, 11, 163. [PubMed: 19152152]

[40]. Irie K, Ejiri S, Sakakura Y, Shibui T, Yajima T, The journal of histochemistry and cytochemistry : official journal of the Histochemistry Society 2008, 56, 561. [PubMed: 18319272]

[41]. Gomes PS, Fernandes MH, Laboratory Animals 2011, 45, 14. [PubMed: 21156759]

[42]. Lieberman DE, Pearson OM, Polk JD, Demes B, Crompton a W., The Journal of experimental biology 2003, 206, 3125. [PubMed: 12909694]

[43]. Artzi N, Oliva N, Puron C, Shitreet S, Artzi S, bon Ramos A, Groothuis A, Sahagian G, Edelman ER, Nature materials 2011, 10, 704. [PubMed: 21857678]

[44]. Artzi N, Shazly T, Baker AB, Bon A, Edelman ER, Advanced Materials 2009, DOI 10.1002/adma.200900340.

[45]. Shrivastava PK, Singh R, Shrivastava SK, Chemical Papers 2010, DOI 10.2478/s11696-010-0042-6.

[46]. Unterman S, Charles LF, Strecker SE, Kramarenko D, Pivovarchik D, Edelman ER, Artzi N, ACS Nano 2017, 11, 2598. [PubMed: 28221760]

[47]. Sharma A, Meyer F, Hyvonen M, Best SM, Cameron RE, Rushton N, Bone & Joint Research 2012, 1, 145. [PubMed: 23610684]

[48]. Suliman S, Xing Z, Wu X, Xue Y, Pedersen TO, Sun Y, Døskeland AP, Nickel J, Waag T, Lygre H, Finne-Wistrand A, Steinmüller-Nethl D, Krueger A, Mustafa K, Journal of Controlled Release 2015, 197, 148. [PubMed: 25445698]

[49]. Faßbender M, Minkwitz S, Strobel C, Schmidmaier G, Wildemann B, International Journal of Molecular Sciences 2014, 15, 8539. [PubMed: 24830556]

[50]. Patel JJ, Flanagan CL, Hollister SJ, Tissue Engineering Part C: Methods 2014, DOI 10.1089/ten.tec.2014.0377.

[51]. Srouji S, Livne E, in Mechanisms of Ageing and Development, 2005, pp. 281–287. [PubMed: 15621208]

[52]. a Puleo D, Huh WW, Duggirala SS, DeLuca PP, J Biomed Mater Res 1998, 41, 104. [PubMed: 9641630]

[53]. Crisera F, Warren S, Greenwald J, Spector J, Peled Z, Bouletreau P, Longaker M, Craniofacial Surgery 9 2001.

[54]. Por YC, Barceló CR, Salyer KE, Genecov DG, Troxel K, Gendler E, Elsalanty ME, Opperman LA, in Annals of the Academy of Medicine Singapore, 2007, pp. 911–919.

[55]. Warren SM, Greenwald JA, Nacamuli RP, Fong KD, Song HJM, Fang TD, Mathy JA, Longaker MT, The Journal of craniofacial surgery 2003.

[56]. Ogle RC, Tholpady SS, McGlynn KA, Ogle RA, in Cells Tissues Organs, 2004

[57]. Soltanoff CS, Yang S, Chen W, Li Y-P, Critical reviews in eukaryotic gene expression 2009, 19, 1. [PubMed: 19191755]

[58]. Reyes R, Rodríguez JA, Orbe J, Arnau MR, Évora C, Delgado A, Drug Delivery 2018, DOI 10.1080/10717544.2018.1446473.

[59]. a Puleo D, Journal of cellular physiology 1997, 173, 93. [PubMed: 9326453]

[60]. Verdelis K, Lukashova L, Atti E, Mayer-Kuckuk P, Peterson MGE, Tetradis S, Boskey AL, van der Meulen MCH, Bone 2011, DOI 10.1016/j.bone.2011.05.013.

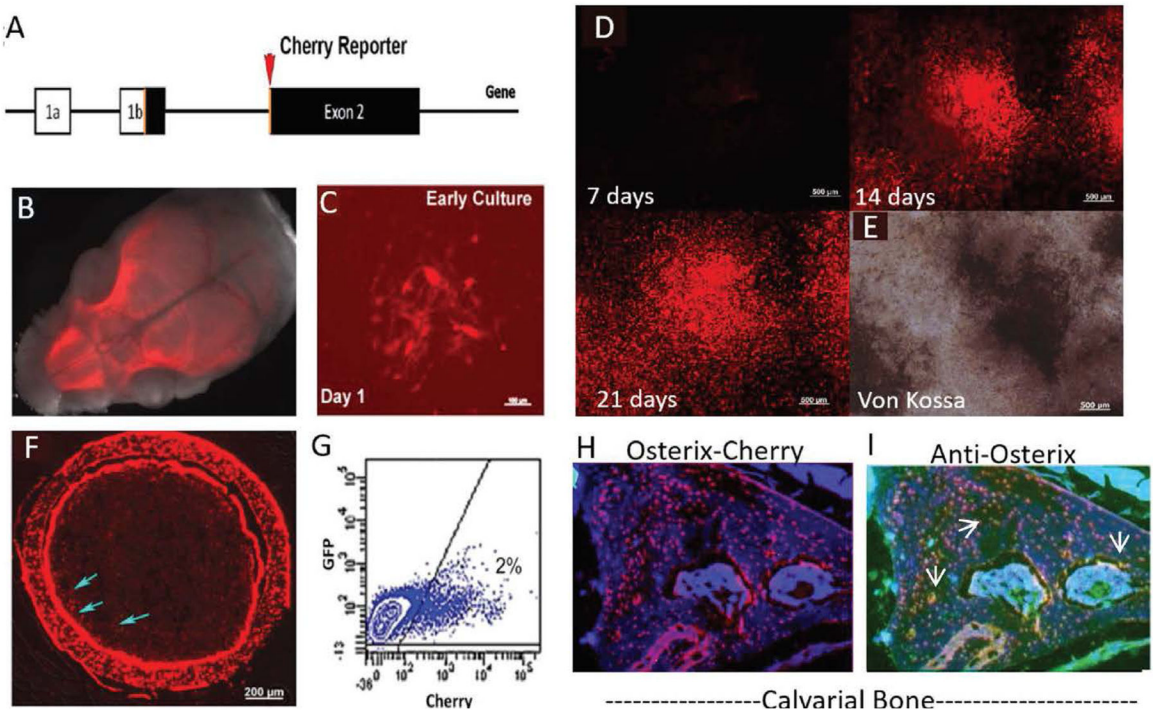


**Figure 1: Osterix-Cherry mice allow for tracking of pre-osteoblastic / mesenchymal cells in vivo.**

(A) Osterix-mCherry reporter construct showing the location of the fluorescent reporter in relation to the translational start site. (B) Whole mount skull from P2 Osterix-mCherry reporter mouse indicating fluorescence is localized to skeletal tissue. (C) Culture of bone marrow stromal cells (BMSC), showing colonies of mCherry cells after 24 hours in vitro (scale bar = 50μm). (D) Time course of BMSC culture with consistent 15ms exposure time confirming increasing brightness of colonies (scale bar = 500μm). (E) Mineralization by von Kossa at 21 days correlating with bright Osterix-mCherry expression (scale bar = 500μm). (F) Cortical section showing Osterix-mCherry expression within Osteoblasts, Osteocytes and mesenchymal stem cells (blue arrows) (scale bar = 200μm). (G) Flow of freshly isolated bone marrow showing 2% of the cells are positive for mCherry expression. (H) Calvarial section showing Osterix-mCherry expression within the bone. (I) Same calvarial section seen in H, immunostained for Osterix using a green secondary antibody, showing co-localization with H (white arrows, yellow cells).

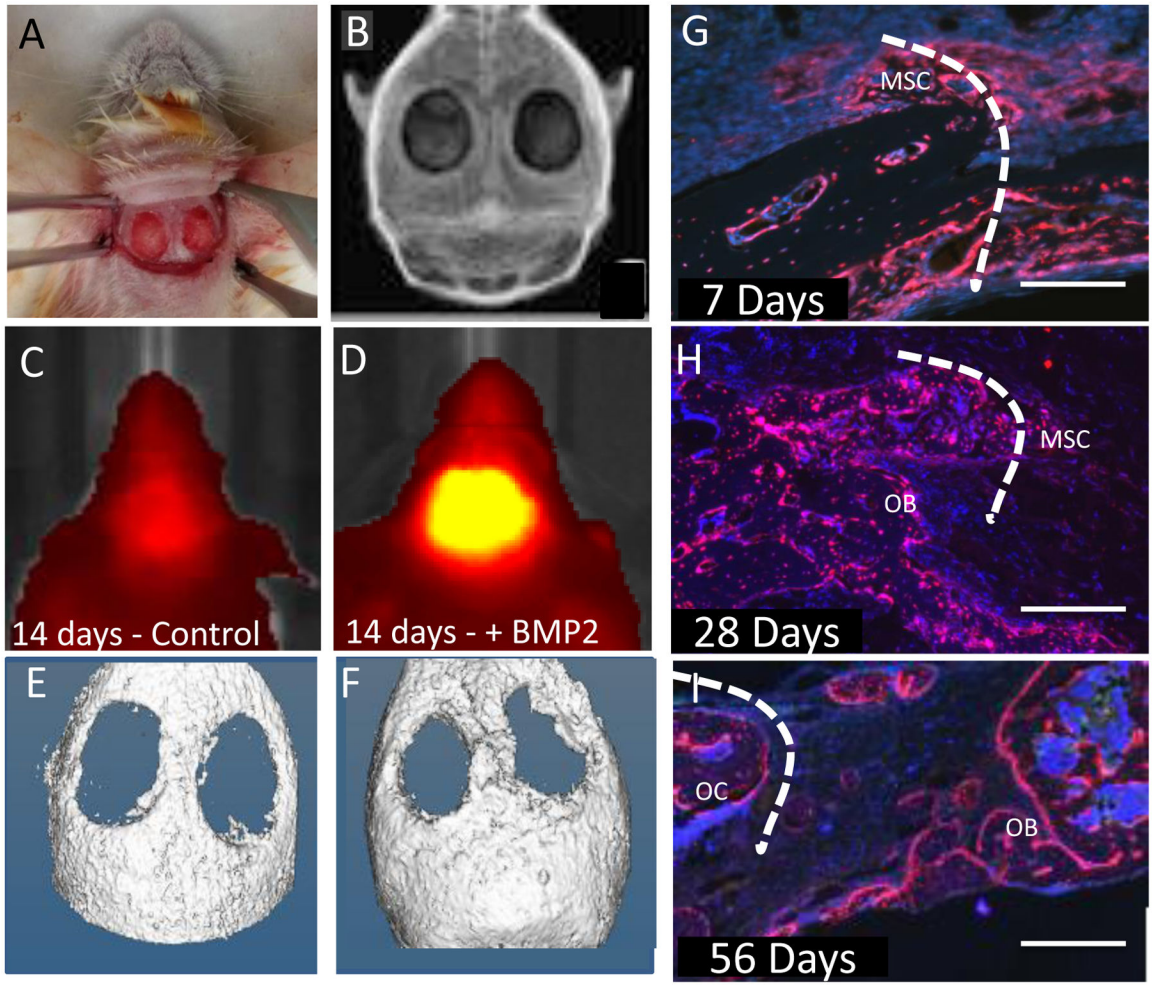


**Figure 2: Osterix-Cherry expression provides a read out of putative bone formation before mineralization and correlating with neo-osteogenesis.**

(A) Osterix mCherry mouse prepared for insertion of either collagen sponge or nanocomposite hydrogel. (B) X-ray of bilateral calvarial defect post surgery. (C) Osterix-mCherry mouse IVIS image 14 days post surgery with only collagen sponge inserted. (E) Corresponding μCT image. (D) Osterix-mCherry mouse IVIS image 14 days post surgery with collagen sponge infused with rhBMP-2. (F) Corresponding μCT image. (G) Calvarial defect treated with a collagen sponge infused with rhBMP-2 7 days post surgery showing mesenchymal stem cells (MSC) infiltrating the defect site (scale bar = 500μm). (H) Calvarial defect treated with a collagen sponge infused with rhBMP-2 28 days post surgery showing MSCs and Osterix-mCherry Osteoblasts (OB) (scale bar = 500 μm). (I) Calvarial defect treated with a collagen sponge infused with rhBMP2 56 days post surgery showing Osterix-mCherry Osteoblasts (OB) and Osteocytes (OC) (scale bar = 500 μm). Dotted line represents defect edge.

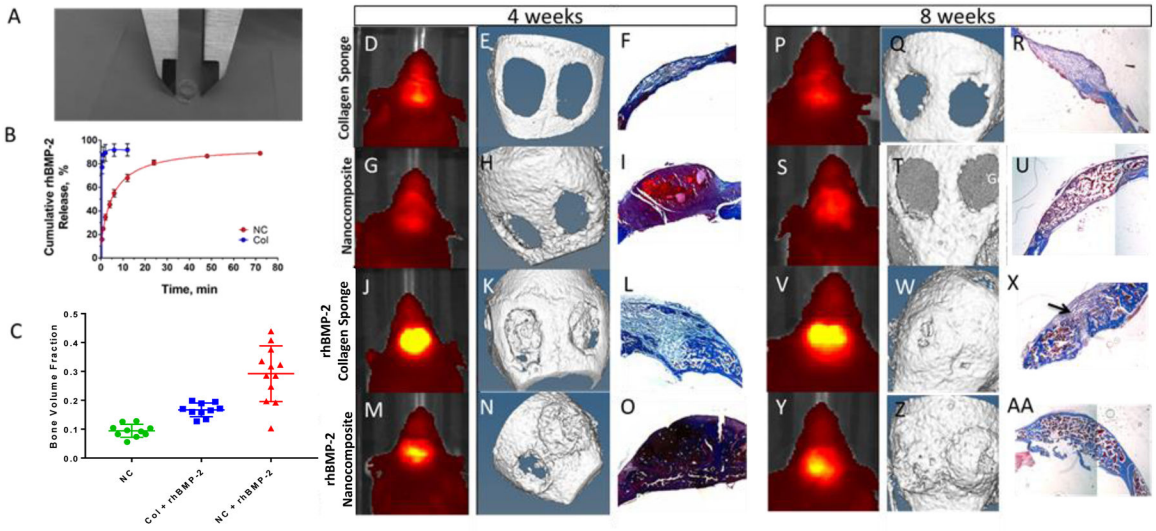


**Figure 3: rhBMP-2 loaded material stimulates mineralization and bone volume fraction at 4 and 8 weeks.**

(A) 6mm nanocomposite hydrogel formed in a mold. (B) Release of fluorescently tagged rhBMP-2 from nanocomposite (red, NC) or collagen sponge (blue, Col) n=3. (D, G, J, M, P, S, V, Y) IVIS imaging of a representative mouse. (E, H, K, N, Q, T, W, Z) μCT imaging of a representative mouse. (F, I, L, O, R, U, X, AA) Masson's Trichrome staining of a representative tissue section. Orange arrows show nanocomposite material in the defects. Black arrow indicates incomplete bridging. n=10 (C) Bone volume fraction (BV/TV) for treated groups (blue; collagen sponge with rhBMP-2, green; nanocomposite, red; nanocomposite with rhBMP-2) n=10, ** $p<0.05$

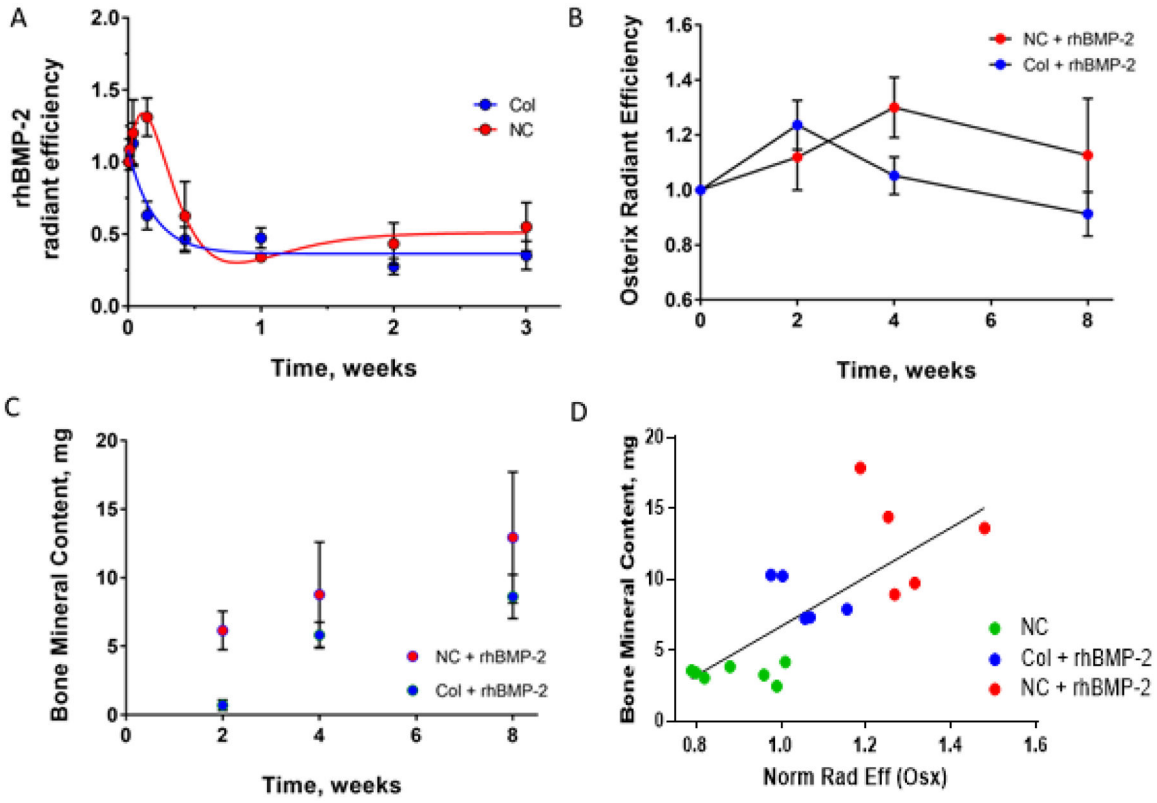


**Figure 4: Osterix-mCherry expression correlates with final bone mineral content.**

A) Fluorescently labeled rhBMP-2 release *in vivo* showing an initial burst in both nanocomposite (red, NC) and collagen sponge (blue, Col) with prolonged release of rhBMP-2 in the nanocomposite group B) Radiant efficiency of Osterix-mCherry as measured by IVIS over time post surgery (blue; collagen sponge with rhBMP-2, red; nanocomposite with rhBMP-2) indicating a response of these fluorescently labeled cells C) Bone mineral content over time as measured via μCT (blue; collagen sponge with rhBMP-2, red; nanocomposite with rhBMP-2) showing equivalent bone formation in both groups D) Correlation between final bone mineral content at 8 weeks and radiant efficiency as measured by IVIS at 4 weeks. (blue; collagen sponge with rhBMP-2, green; nanocomposite, red; nanocomposite with rhBMP-2) For nanocomposite, n=6, for all other groups n=5. This is equivalent to 12 defects in the nanocomposite group and 10 defects in the other groups. ** $p<0.05$

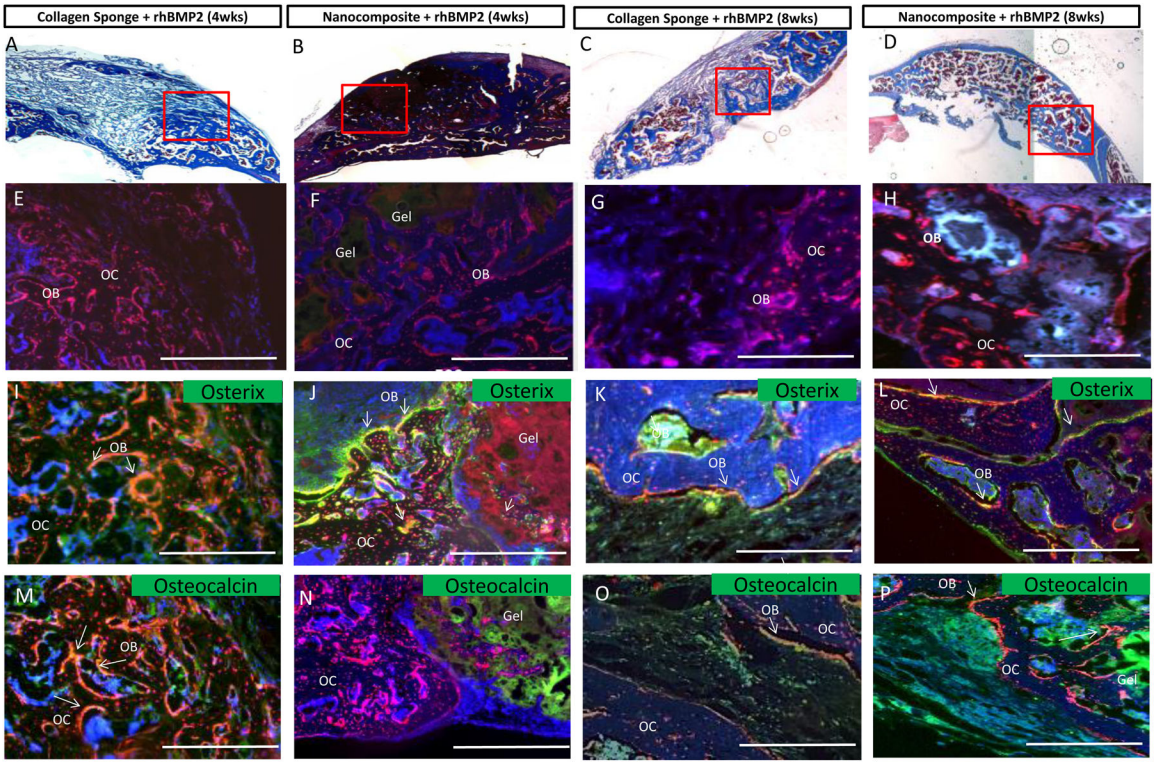


**Figure 5: rhBMP-2 loaded materials stimulate Osterix and Osteocalcin expression at 4 and 8 weeks**

(A) Collagen sponge treated with rhBMP-2 implanted for 4 weeks; (B)Nanocomposite treated with rhBMP-2 implanted for 4 weeks; (C) Collagen Sponge treated with rhBMP-2 implanted for 8 weeks; (D) Nanocomposite treated with rhBMP-2 implanted for 8 weeks. A, B, C, and D show Masson's Trichrome staining and the red boxes indicate the area of interest shown in subsequent sections. Collagen deposition stained in blue. E, F, G and H images show endogenous Osterix expression as red fluorescence. DAPI is shown in blue. I, J, K, and L images show endogenous Osterix expression in red and immunostaining for Osterix in green. M, N, O, and P images show endogenous Osterix expression in red and areas of osteocalcin immunostaining in green. Overlap in all images is seen in yellow and marked with white arrows, marking the bone surface. The nanocomposite hydrogel has a distinct physical appearance and is marked. Scale bars=500mm. Gel = Nanocomposite hydrogel; OB= Osteoblasts; OC=Osteocytes.